# Surface charging of dielectric barriers in short rod-plane air gaps – experiments and simulations

Hans Kristian Meyer*, Andreas Blaszczyk†, Michael Schueller‡, Frank Mauseth* and Atle Pedersen§

*NTNU – Norwegian University of Science and Technology, Trondheim, Norway
†ABB Ltd., Baden-Dättwil, Switzerland
‡University of Applied Sciences Rapperswil, Institute for Energy Technology, Switzerland
§SINTEF Energy Research, Trondheim, Norway

*Abstract*—Surface charge on dielectric surfaces can alter the field conditions of insulation systems substantially. In this work, lightning impulse experiments are compared with a simulation model for surface charging in rod-barrier-plane geometries. The model is based on the saturation charge assumption, i.e. zero normal electric field in air pointing onto the dielectric surface, which prevents further charging. This hypothesis holds well for most geometries, as long as there are no leader discharges or restrikes (also known as back discharges). Restrikes are discharges that occur on the lightning impulse tail when the active electrode is close to zero potential. A method is proposed to compute the charge distribution after a restrike. Furthermore, the model can predict discharges on both sides of the barrier. Saturation charge fields can be computed efficiently, so the results are encouraging for dielectric design applications.

## I. Introduction

Accurate modelling of surface charging phenomena is important for the development of $SF_6$-free insulation systems for the next generation of medium voltage switchgear. Discharges can be tolerated during lightning impulse tests as long as they do not lead to breakdown. Surface charging effects can suppress discharges under such conditions. In this work, experiments are compared with variations of the saturation charge model described in [1]. Lightning impulses are applied to rod-plane air gaps with a dielectric barrier (see fig. 1), and the resulting surface potential is measured. A range of short ($< 100$ mm) rod-barrier-plane geometries are used to test the model and obtain an overview of the charging phenomena involved.

## II. Experiments

### A. Voltage and current

Rod-barrier-plane gaps (fig. 1 and table I) were stressed with $1.2/50$ μs lightning impulses (LI). The earth current was monitored using a Pearson 6585 current monitor to ensure that there was a discharge. No breakdowns were observed.

### B. Surface potential measurements

A Trek 3455ET probe with a 20 kV Trek 341B high voltage amplifier was used to measure surface potential after a discharge. The probe zeroes the electric field between itself
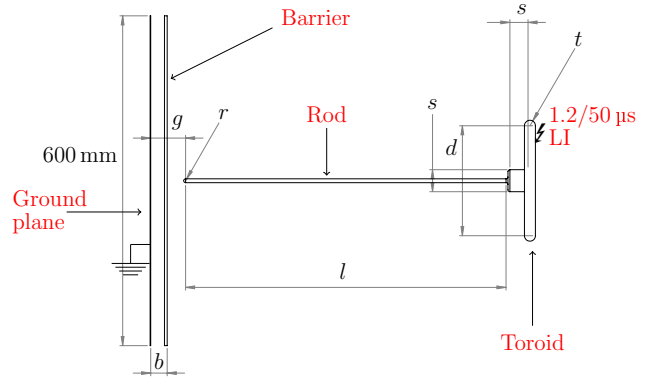
Fig. 1. Rod-barrier-plane model. See table I for parameters. The Lexan barrier was 600x600x5 mm, the ground plane of 600x1000x1 mm. Toroid dimensions: $d = 200$ mm, $t = 20$ mm, $s = 40$ mm.

TABLE I
ROD-BARRIER-PLANE CONFIGURATIONS IN THIS WORK (SEE FIG. 1 FOR PARAMETER ILLUSTRATION)

| Parameter | Configuration | | | | | |
|---|---|---|---|---|---|---|
| | 1 | 2 | 3 | 4 | 5 | 6 |
| $g$ [mm] | 15 | 20 | 10 | 60 | 35 | 60 |
| $b$ [mm] | 5 | 15 | 5 | 5 | 15 | 40 |
| $r$ [mm] | 3.5 | 3.5 | 2 | 3.5 | 3.5 | 3.5 |
| $l$ [mm] | 590 | 590 | 288 | ca. 600 | 590 | ca. 600 |
| $V$ [kV] | 35 | −50 | 35 | 54 | ±50 | −100 |

and the surface by adjusting its potential. After the impulse, the barrier and ground plane were moved along a rail and positioned 5 mm ± 3 mm from the probe tip. The surface potential on the barrier was then scanned along the center line using a robot stage. In some cases a 2D raster scan was also performed. The barrier was subsequently cleaned with isopropyl alcohol before the next experiment, resulting in a residual surface potential magnitude below 300 V.

Local potential differences smaller than the surface area seen by the probe are not resolved [2]. This circular area can be assumed to be around 6–18 mm diameter [3]. Local charge peaks or sharp gradients are therefore smoothened. To mimic this effect in the simulations, a moving average filter was applied. While the robot is scanning the surface with a speed of 30 mm s$^{-1}$, the surface potential values are sampled

with 100 samples/s. The moving average filter averages 50 samples, which corresponds to a resolution of $15\,\mathrm{mm}$.

## C. Measurements on both barrier sides

In some negative impulse configurations (5 and 6 in table I), multiple discharge events were observed on the measured current, and it was suspected that there could be positive streamers between the barrier and the ground plane (as observed in [4]). To initiate such discharges repeatably, a small protrusion (ca. $1\,\mathrm{mm}$ radius copper wire protruding ca. $2\,\mathrm{mm}$) was placed on the ground plane. In addition to the initial surface potential measurement, the barrier was turned around carefully to measure the surface potential on the side that was hypothetically charged by positive streamers starting from the protrusion. Consequently, the side with negative charge delivered from the rod was facing the ground plane during this second measurement.

## III. SIMULATIONS

First principles simulations of electrical discharges (see e.g. [5]) are still too computationally heavy to be used in everyday insulation design. Simplified calculations are therefore needed. One approach is to assume that surfaces exposed to discharges are charged to saturation, i.e. that the normal electric field component vanishes at the surface facing the air [1].

The advantage with this method is that it can be quickly calculated for arbitrary 3D and 2D geometries. The calculation procedure used in this work is as follows (see also fig. 2 and 3):

1) Calculate background field with zero surface charge and applied voltage $U$.
2) Evaluate discharge propagation paths (as field lines) and the streamer inception voltage $U_i$ .
3) If a streamer collides with a dielectric surface, assume on an area $A_\sigma$ of this surface the saturation charge boundary condition and compute the unknown saturation charge $\sigma_{\mathrm{sat}}$ according to (1) and (2). The outer border of $A_\sigma$ is determined from the maximum streamer propagation range calculated as applied voltage $U$ divided by the stability fields $E_{\mathrm{st},+} = 0.5\,\mathrm{kV\,mm^{-1}}$ for positive and $E_{\mathrm{st},-} = 1\,\mathrm{kV\,mm^{-1}}$ for negative polarities.
4) Calculate saturation inception voltage $U_{\mathrm{i,sat.}}$. If $U_{\mathrm{i,sat.}} > U$, scale down $U$ until $U_{\mathrm{i,sat.}} = U$. For the reduced voltage the discharge, and therefore also the surface charging, will be suppressed.
5) Evaluate whether there are new critical field lines that will lead to inception and charging of other surfaces.
6) Ground the active electrode and calculate restrike inception voltage $U_{\mathrm{i,res}}$. For $U_{\mathrm{i,res}} \leq U$, the prediction is that there will be restrikes between the dielectric surface and the electrode when it is grounded.
7) If there is a restrike, remove a fraction of the surface charge and calculate the new shape assuming that the normal field is equalized in the region where charge is removed. Change the fraction iteratively until the restrike is suppressed, i.e. $U \leq U_{\mathrm{i,res}}$.
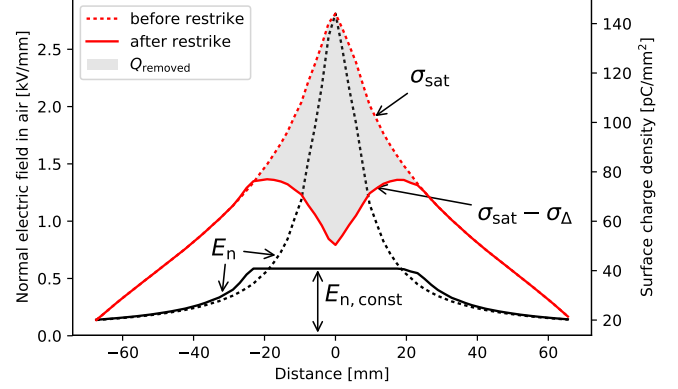


Fig. 2. Charge density and normal field distributions before and after a simulated restrike. The presented values correspond to the configuration 3 in table I. The value of $Q_{\mathrm{removed}}$ is equal to $5\,\%$ of the total saturation charge and has been estimated iteratively so that $U = U_{\mathrm{i,res}}$.

8) Recalculate the field without the active electrode and extract the surface potential for comparisons with experiments.

The following equations are formulated for a point $j$ representing a surface element affected by charging

$$E_{\mathrm{n,air},j} - E_{\mathrm{n,const}} = 0 \tag{1}$$

$$\epsilon_{\mathrm{ins}}E_{\mathrm{n,ins},j} + \sigma_{\Delta,j} - \epsilon_{\mathrm{air}}E_{\mathrm{n,const}} = \sigma_{\mathrm{sat},j} \tag{2}$$

$$\Sigma S_j \sigma_{\Delta,j} = Q_{\mathrm{removed}} \tag{3}$$

These equations allow computation of the "volcano"-shaped surface charge distribution after a restrike, as shown in fig. 2. $S_j$ is the surface area of a surface element $j$ and $\sigma_{\Delta,j}$ is the charge density removed for this element. $E_{\mathrm{n,const}}$ is an unknown value of the equalized normal field onto the surface. $\sigma_{\mathrm{sat},j}$ is the saturation charge accumulated on the surface element $j$ before the restrike occurred. $Q_{\mathrm{removed}}$ is the total removed charge by a restrike, see fig. 2. For the computation of saturation charge, only equations (1) and (2) are used where $E_{\mathrm{n,const}}$ and $\sigma_{\Delta,j}$ are set to zero. $\sigma_{\mathrm{sat},j}$ is then moved to the left side of (2) since it is an unknown quantity.

The barrier turning procedure described in sect. II-C was also reproduced in the simulations for comparisons.

## IV. RESULTS AND DISCUSSION

### A. Agreement with saturation charge

The measured surface potential shape is generally close to the simulated potential distribution, see fig. 4. There is some spread within each configuration.

It is often seen that the discrepancy is highest at the center. This is mainly because of *restrikes* (also called back discharges), which create a "volcano" shape. The discharges have previously been observed by the authors as pulses with some $100\,\mathrm{kHz}$ at the tail of the lightning impulse [3]. Five other tested configurations, not included in table I, show similar agreement with the simulation model.
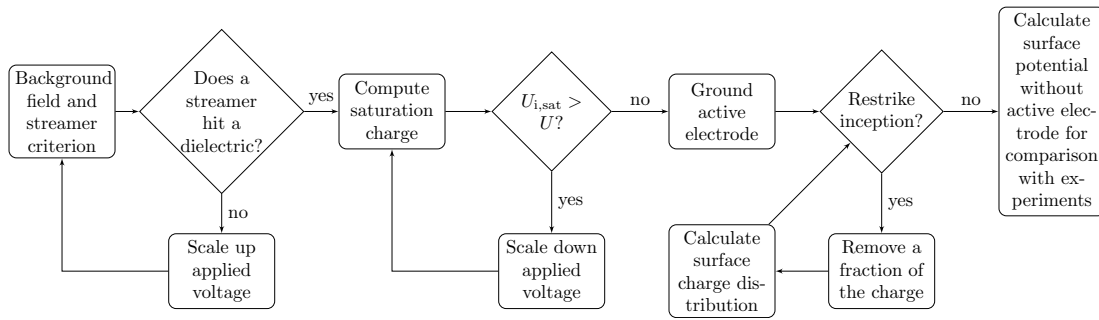
Fig. 3. Flow chart for calculating surface charge distributions, see sect. III.
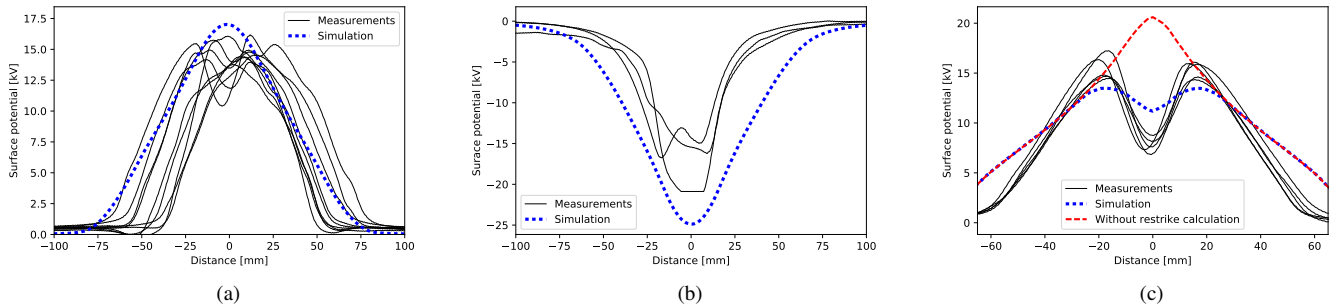


(a)      (b)      (c)

Fig. 4. The surface potential measured (solid lines) and simulated (dotted and dashed lines) for: a) configuration 1. b) configuration 2, c) configuration 3 (table I for details on the configurations). Due to inception suppression, the simulation voltage has been reduced to 93 % in a). Both the saturation stage and restrike stage computations are shown in c).

The surface charge density distribution variation is primarily due to the following factors:

- Statistical time lag for inception and the stochastic nature of discharge propagation. The effect is especially strong when the inception occurs after the lightning impulse peak.
- Time lag between the impulse and the measurement – this time varied within the range of 2-3 minutes. Ideally the results should be corrected with a decay coefficient that can be found from fig. 6.
- Measurement and positioning errors, which are in the range of 2-3 mm in this work.

### B. Charging by leaders

Leaders will charge the surface to a greater extent [6]. This was observed in experiments partly published in [3], see fig. 5. There, the leader discharge leads to higher surface potential than predicted by the simulation model.

As the leader is highly conductive, it can approximately be considered as an extension of the HV electrode. A new saturation charge computation might then give a better fit with the measured charge distribution.

### C. Surface potential decay

As can be seen in fig. 6, the potential decays within a couple of hours. When the probe was left near the surface, the decay was slowed down substantially. The probe was therefore moved away between measurements.
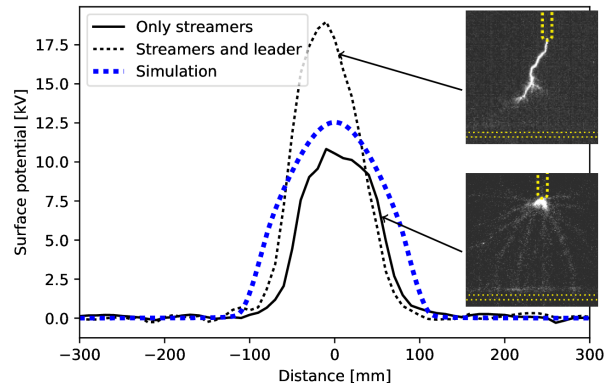


Fig. 5. Leader discharges cause charging above background field saturation charge. Surface potential along the center line and saturation charge after a leader-less discharge. The measurements are taken from a previous publication where a high-speed camera was also used [3]. Image of the discharge with only streamers and image of the measured discharge with an arrested leader inset. Barrier and rod position indicated with dotted yellow lines. Configuration 4 (see table I).

As the probe was seen to halt the decay, it seems plausible that the probe stops neutralization by gas ions. The potentials measured are probably slightly lower than those seen during the discharge, as it took around two minutes to move the barrier to the measurement position.
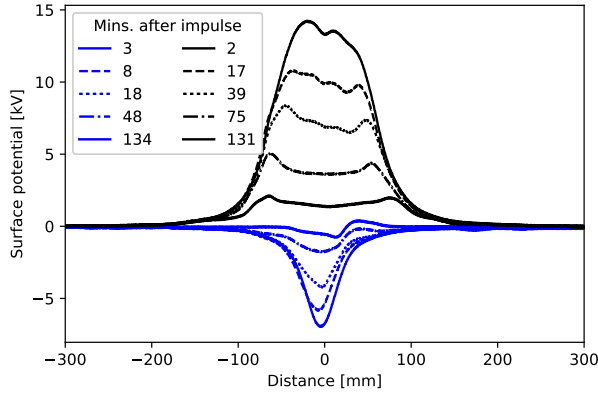
Fig. 6. The surface potential disappears almost completely within two hours. Configuration 5 (see table I). Decay after both a positive and a negative impulse are shown. Interestingly, the amount of charge is smaller for the negative than for positive impulse (at the same applied voltage). This can be explained by larger stability field required for negative streamers to propagate.

### D. Restrike prediction

Although there are likely restrikes in several of the measurements in fig. 4, the restrike shape was only computed for one geometry, shown in fig. 4c.

### E. Discharges on both sides

Discharges on both sides of the barrier have been previously observed by the authors with a high-speed camera (see fig. 7e and [4], [7]). Experimental scans and simulation of the surface potential on both sides of the barrier after such an event are presented in fig. 7a to 7d.

On the rod side, fig. 7a and 7c, the surface potential is, as expected, negative (similar to the result in fig. 4b). More surprising is the potential distribution on the opposite side (after turning the barrier). There is a significant positive potential in the middle, which confirms the existence of the positive charge. However, the positively charged area is limited since it is surrounded by a negative potential originating from the negative charge on the other barrier side. The simulation, fig. 7d, could well reproduce the trends observed in experiment, fig. 7b. It should be noted that the measurement in fig. 7a was partly out of the probe range (which is ca. 21 kV), so the prediction in fig. 7c could not be reached.

## V. CONCLUSION

This work presents experiments and simulations of charging of a dielectric barrier in rod-plane gaps under lightning impulse stresses. The experimental results are compared with a simulation model based on the assumption of zero normal electric field on the dielectric surface. The model is extended to predict the influence of restrikes and discharges on both sides of the barrier. There is, in general, good agreement between experiments and simulations. The simulation model is computationally inexpensive and applicable to real-life switchgear insulation systems. The reader is referred to [8] for details about the software architecture.
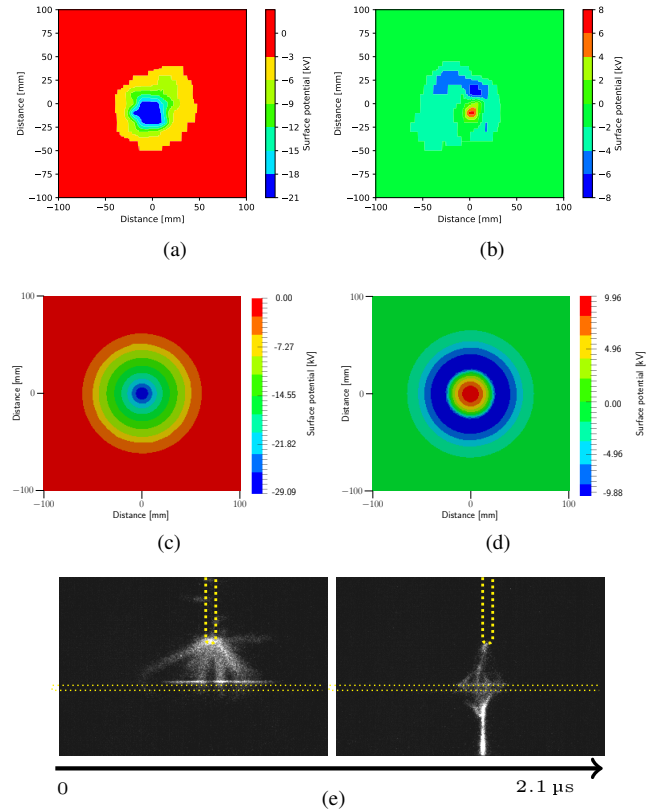


(a)

(b)

(c)

(d)

(e)

Fig. 7. Discharges on both sides. Configuration 2, with a small protrusion placed centrally on the ground plane to provoke a discharge on the ground side. a) measured on the rod side, b) barrier turned and measured. c) and d) simulations (corresponding to a) and b)) respectively. e) High speed image example of discharge development from both the rod and the ground plane (configuration 6, previously published in [7]). Barrier and rod position indicated with dotted yellow lines. Camera frame timing also indicated.

## REFERENCES

[1] A. Pedersen and A. Blaszczyk, "An engineering approach to computational prediction of breakdown in air with surface charging effects," *IEEE Transactions on Dielectrics and Electrical Insulation*, vol. 24, no. 5, pp. 2775–2783, Oct. 2017.

[2] M. A. Noras, "Non-contact surface charge/voltage measurements: capacitive probe—principle of operation," *Trek Application Note*, no. 3001, pp. 1–8, 2002.

[3] H. K. Meyer, F. Mauseth, M. Husøy, and A. Pedersen, "Surface charging of dielectric barriers under positive lightning impulse stress," in *2017 IEEE Conference on Electrical Insulation and Dielectric Phenomenon (CEIDP)*, Oct. 2017, pp. 802–806.

[4] H. K. Meyer, F. Mauseth, A. Pedersen, and J. Ekeberg, "Breakdown mechanisms of rod-plane air gaps with a dielectric barrier subject to lightning impulse stress," *IEEE Transactions on Dielectrics and Electrical Insulation*, vol. 25, no. 3, pp. 1128–1134, Jun. 2018.

[5] A. A. Dubinova, "Modeling of streamer discharges near dielectrics," Ph.D. dissertation, TU Eindhoven, 2016.

[6] J. Deng, H. Mu, G. Zhang, S. Matsuoka, A. Kumada, and K. Hidaka, "Residual Charge Distribution of Surface Leader Discharge Under Positive Impulse Voltage," *IEEE Transactions on Plasma Science*, vol. 41, no. 4, pp. 999–1004, Apr. 2013.

[7] M. Husøy, "Streamer Charging of Dielectric Barriers in Inhomogeneous Air Gaps," Master's thesis, NTNU, Jun. 2017.

[8] A. Blaszczyk, J. Ekeberg, S. Pancheshnyi, and M. Saxegaard, "Virtual High Voltage Lab," in *Scientific Computing in Electrical Engineering - SCEE 2016*, ser. Mathematics in Industry, U. Langer, W. Amrhein, and W. Zulehner, Eds. Heidelberg: Springer, 2018.